Surface Functionalization of "Rajshahi Silk" Using Green Silver Nanoparticles

Sakil Mahmud [1,2,*], **Mst. Zakia Sultana** [1,3], **Md. Nahid Pervez** [1,4] iD, **Md. Ahsan Habib** [1,5] and **Hui-Hong Liu** [1,*] iD

[1] School of Chemistry and Chemical Engineering, Wuhan Textile University, Wuhan 430200, China; zakia1136@gmail.com (M.Z.S.); mp58@hw.ac.uk (M.N.P); habibitltd@gmail.com (M.A.H.)

[2] Ningbo Institute of Material Technology and Engineering, Chinese Academy of Sciences, Ningbo 315201, China

[3] NUS Graduate School for Integrative Science & Engineering, National University of Singapore, 28 Medical Drive, Singapore 117456, Singapore

[4] Research Institute of Flexible Materials, School of Textiles & Design, Heriot-Watt University, Galashiels TD1 3HF, UK

[5] Institutes of Chemistry, Chinese Academy of Sciences, Beijing 100190, China

[*] Correspondence: sakilhabib@gmail.com (S.M.); huihongliu@wtu.edu.cn (H.-H.L.); Tel.: +86-131-1665-5691 (S.M.); +86-150-7136-6519 (H.-H.L.)

Abstract: In this study, a novel functionalization approach has been addressed by using sodium alginate (Na-Alg) assisted green silver nanoparticles (AgNPs) on traditional "Rajshahi silk" fabric via an exhaustive method. The synthesized nanoparticles and coated silk fabrics were characterized by different techniques, including ultraviolet–visible spectroscopy (UV–vis spectra), scanning electron microscopy (SEM), transmission electron microscopy (TEM), energy dispersive X-ray spectroscopy (EDS), X-ray diffraction (XRD), thermogravimetric analysis (TGA), and Fourier transform infrared spectroscopy (FT-IR), which demonstrated that AgNPs with an average size of 6–10 nm were consistently deposited in the fabric surface under optimized conditions (i.e., pH 4, temperature 40 °C, and time 40 min). The silk fabrics treated with AgNPs showed improved colorimetric values and color fastness properties. Moreover, the UV-protection ability and antibacterial activity, as well as other physical properties—including tensile properties, the crease recovery angle, bending behavior, the yellowness index, and wettability (surface contact angle) of the AgNPs-coated silk were distinctly augmented. Therefore, green AgNPs-coated traditional silk with multifunctional properties has high potential in the textile industry.

Keywords: silver nanoparticles; silk; functional finishing; wettability; surface modification

1. Introduction

In recent years, nanoparticles have generated great interest in different fields, including chemistry, physics, materials science, life sciences, and engineering due to their superior properties; for example, optical, magnetic, electronic and catalytic properties [1]. Among metallic nanoparticles (NPs), the size of AgNPs ranges between 1 nm and 100 nm, making them one of the best candidates for several applications including biosensing, antibacterial, antiviral, and antifungal activities, drug delivery, catalysis, electrochemical, conductivity [2,3], and so on, with exponential accretion production. Generally, a number of physical and chemical methods are available for the preparation of metal NPs [4,5], which are not environmentally friendly. Recently, the ever-increasing interest has been amplified by requests for "green" synthesis methods [6]. Therefore, knowledge of current

environmental issues is considered to be the present motivation for the green synthesis of nanoparticles. Ideally, the synthesis of nanoparticles from a green chemistry perspective is associated with three main points: the choice of the solvent medium, use of an environmentally benign reducing agent, and a source of nontoxic material for the stabilization of the nanoparticles. Some researchers have reported the green preparation of nanoparticles through natural polymers like chitosan, soluble starch, polypeptide, heparin, and hyaluronan used as reducing and stabilizing agents [7]. Recently, polysaccharide-based materials have been associated with the synthesis of green AgNPs through the use of an eco-friendly benign solvent; i.e., using water and polysaccharides as capping agents [8]. Sodium alginate is a type of polysaccharide polymer that is isolated from marine algae and consists of β-D-mannuronic (M) and its stereoisomer α-L-guluronic (G) acid that forms a kind of linear block copolymer of branched chains. It is ideal for use due to its excellent cytocompatibility and biocompatibility, biodegradation, sol–gel transition properties, and chemical versatility that makes it more viable in terms of making modifications to tailor its properties [9,10]. A number of free hydroxyl and carboxyl groups from its backbone allow it to dissolve well in water due to a negatively-charged carboxyl group. In the synthesis of sodium alginate (Na-Alg)-assisted AgNPs, the reaction between Na-Alg and Ag^+ possibly leads to the formation of a Na-Alg complex $[Ag\,(Na\text{-}Alg)]^+$, which is responsible for the formation of AgNPs by silver ion reduction in the presence of alginic acid regeneration. Darroudi et al. reported that using glucose can reduce silver ions to metallic silver to form AgNPs, and through this process it is oxidized to glucolic acid [11]. The better stability of alginates compared to chitosan has been well documented due to their noteworthy properties, such as being water-soluble that covers gel formation in the absence of heating or cooling, and also playing a pivotal role in trapping molecules—which remain free to migrate by diffusion, depending on their size—through capillary forces. These features make alginates ideal for the stabilization of AgNPs in order to fulfill the demand of the eco-friendly or green synthesis approach. Nowadays, the modification of silk material with AgNPs has attracted a good deal of interest for diverse applications in the clinical, safety, and production engineering, water technology, clothing, lightweight creation, and automotive industries [12].

Rajshahi silk is the name given to the silk produced in Rajshahi, Bangladesh. It is a famous name in the clothing and textiles sector. Although the situation of the Bangladesh textile market is presently dominated by synthetic products, the charming features of Rajshahi silk allow it to maintain its celebrated position [13]. Rajshahi silk is an aerial and bendable fiber produced from the cocoons of silkworms, and is covered with a protein known as sericin that has been commonly used in textiles for thousands of years due to its inherent luster, notable flexibility, environmental friendliness, and exquisite mechanical strength [14]. Analysis of the chemical structure of silk reveals that the sericin protein is composed of 18 amino acids that—most importantly—have sturdy polar moieties which include hydroxyl, carboxyl, and amino groups that are sufficient to bind charged functional institution of natural or inorganic substances. As a natural protein fiber, silk possesses a structure similar to human skin with easy, breathable, tender, non-itchy, and antistatic characteristics. The occurrence of these distinct properties makes silk an ideal material for the selective adhering of metal ions [15].

However, research around the advancement of "Rajshahi silk" fiber properties in order to retain their traditional position through a functionalization approach is limited. To the best of our knowledge, this is the first report of the surface treatment on Rajshahi silk fabric with green-synthesized AgNPs by using Na-Alg as both a reducing and stabilizing agent. Data from the fabrics treated with this method have been noted in detail in this study.

2. Materials and Methods

2.1. Materials

The mulberry silk fabric was collected from the Bangladesh Sericulture Research and Training Institute (BSR and TI), Rajshahi, Bangladesh. The materials used to synthesize AgNPs were
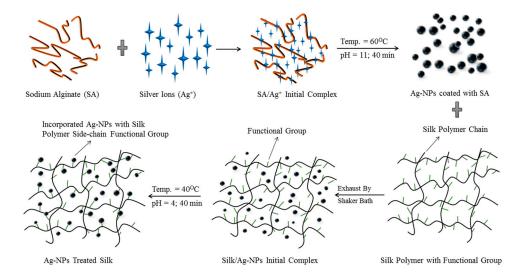
AgNO$_3$ (Shanghai Zhanyun Chemical Co., Ltd., Shanghai, China), sodium alginate (Mw ~ 68,000 Da. Qingdao Yingfei Chemical Co., Ltd., Qingdao, China), and sodium hydroxide (Sinopharm Chemical Reagent Co., Ltd., Beijing, China). Nonionic commercial detergents were used to wash the silk sample. These materials were used throughout the experiment without further purification by using deionized water.

2.2. Green Synthesis of Silver Nanoparticles

A typical synthesis of green AgNPs was accomplished by using an indigenous protocol put together in our laboratory. In brief, 1 mm of AgNO$_3$ was prepared from silver nitrate salt and 1% *w/v* of Na-Alg was prepared with deionized water. NaOH solution was prepared by dissolving NaOH (0.399 g) in deionized water (100 mL). Typically, 1 mL of Na-Alg (1% *w/v*) solution was dropped in 4 mL of silver nitrate (0.001 m) solution with the addition of NaOH solution (approximately 1 mL of 0.01 m) to maintain a pH of 11 in order to accelerate the reaction. These mixtures were stirred for 1 min. Then, the mixture was kept in a heat bath (60 °C) for 40 min. The transparent colorless solution became pale yellow and then brownish-red in color, indicating the formation of AgNPs, which was further confirmed by using UV–vis spectra.

2.3. Application of AgNPs to Rajshahi Silk

The degumming of the raw silk through the removal of sericin from the fibroin was carried out according to [16] with minor modifications. Typically, the degumming process was done three times with 0.05% Na$_2$CO$_3$ solution at boiling point for 30 min. Then, the resulting samples were washed with distilled water and dried at room temperature in order to prepare for the subsequent step. Then, the silk fabric was functionalized with the prepared AgNPs through use of an exhaustive method [17]. The important parameters (pH, temperature, and time) of the AgNPs application to silk were observed. The beakers containing silver solutions were kept in a shaker bath. Since the AgNPs' pH is naturally alkaline, the pH was adjusted by adding weak acid, and the temperature was maintained using the thermostat control on the shaker machine. When the optimum conditions (i.e., the pH and temperature of the AgNPs in the bath) were reached, the silk fabric was immersed and treated at 40 °C for 40 min. Finally, the obtained AgNPs-treated samples were placed for drying at room temperature without rinsing. The whole functionalization process is shown in Scheme 1.

Scheme 1. Schematic diagram of silver nanoparticles coating on silk fabric.

2.4. Measurements and Characterization

The UV–vis spectra of silk fabrics with AgNPs were recorded using a UV-2600 spectrophotometer (Shimadzu Corporation, Kyoto, Japan). The morphologies of samples were observed by using a scanning electron microscope (SEM) (JEOL Ltd., Tokyo, Japan) after gold coating. During the SEM test, an energy dispersive X-ray spectroscopy (EDS) (JEOL Ltd., Tokyo, Japan) spectrum was collected to analyze the composition of chemical elements of the prepared samples. Transmission electron microscopy (TEM) (Hitachi H-7600, Tokyo, Japan) was used to study the particle size distribution of the AgNPs. The crystal behavior of samples was obtained using an X-ray diffractometer (XRD) (Bruker D8 ADVANCE, Karlsruhe, Germany). Fourier transform infrared (FT-IR) measurements were taken with a (Bruker Corporation, Tensor 27, Karlsruhe, Germany) set to a normal transmission mode. Analysis of the thermal behavior of samples was performed in a thermo-gravimetric analyzer (TGA) (Mettler-Toledo Corp., Greifensee, Switzerland) at a heating rate of 10 °C/min in a nitrogen atmosphere. The color strength (K/S) and CIELAB color coordinates (under illuminate D_{65} and $10°$ standard observer) values of samples were measured with the help of a Macbeth Color Eye 7000A spectrophotometer (Gretag Macbeth Ltd., Regensdorf, Switzerland). The color fastnesses to light, ISO 105-BO5, and color fastness to washing, ISO 105 E04, were evaluated. The UV protective characteristics of the original and the silver-coated fabrics were determined in accordance with the Australian/New Zealand Standard AS/NZS 4399:1996 by using a UV–visible spectrophotometer. The antibacterial efficiency of the green-synthesized AgNPs in the silk fabrics against *Staphylococcus aureus* ATCC 6538 as Gram-positive and *Escherichia coli* ATCC 8739 as Gram-negative bacteria [18] was determined. The tensile properties of the silk fabrics were tested before and after AgNPs treatment. The crease recovery angle of the samples was determined as per AATCC Test Method 66-2003 using a Sasmira crease recovery tester (SASMIRA, Mumbai, India). The stiffness in terms of the bending length of untreated and AgNPs-treated samples was tested as per AATCC Test Method 115-2005 using a Sasmira stiffness tester (SASMIRA, Mumbai, India). Static contact angles were measured with a Kruss contact angle instrument (DSA 100, Kruss GmbH, Hamburg, Germany) using deionized water droplets (4 mL) at 25 °C. The moisture regained by each sample was measured in standard atmospheric conditions using the ASTMD 2495 test standard.

3. Results and Discussion

3.1. Characterization of AgNPs

In the present investigation, AgNPs were synthesized via a "green" method using a natural biopolymer alginate assisted by heating an aqueous solution of Na-Alg and $AgNO_3$. The preliminary affirmation of nanoparticles formation was ascertained by recording the absorbance of the colloidal suspension with the use of UV–visible spectrophotometer (Shimadzu Corporation, Kyoto, Japan) in the range of 200–700 nm and simple observation for any color change. The solution turned reddish brown in color, indicating the reduction of silver ions and hence acknowledging the synthesis of the desired AgNPs, as shown in (Figure 1A inset). The distinctive colors of AgNPs become apparent due to a phenomenon known as plasmon absorbance. Incident light creates oscillations in the conduction electrons on the surface of the nanoparticles, and electromagnetic radiation is scattered [19]. Figure 1A shows the UV–vis spectra of pure silver nitrate ($AgNO_3$), SA (sodium alginate), and AgNPs. In the presence of Na-Alg, the band at ~301 nm exhibited by $AgNO_3$ in aqueous solution disappears, indicating possible chelation of Ag+ by the OH and COOH groups from the alginate. The Ag^+ chelate produces $Ag°$ on heating. The intensity and role of the shoulder of the alginate spectrum at approximately 290 nm barely shifted, confirming that there were interactions between the polymer and the metallic precursor. The UV–vis spectrum of the Ag-NPs showed a characteristic peak at about 400 nm, assigned to a strong surface plasmon resonance which has been properly documented for various metal nanoparticles with sizes ranging from 2 to 100 nm [20].

For the synthesis of AgNPs, the typically accepted mechanism shows a two-step process; i.e., atom formation and then polymerization of the atoms. In the first step, a portion of metal ions in the solution is reduced by the available reducing groups. The atoms produced which act as nucleation centers and used to catalyze the remaining metal ions in the bulk solution. Compared with other water-soluble polymers, Na-Alg is an anionic polymer with a high charge density; the negatively-charged alginate allows the positively-charged of silver ions to attach themselves in the polymeric chains, which were reduced in presence of reducing groups. The resulting surface negative charge of alginate fragments containing carboxylic groups stabilizes nanoparticles against coalescing with each other due to electrostatic repulsion and steric outcomes [21]. The FT-IR measurements were executed to analyze the functional groups of the material. Figure 1C shows the pure Na-Alg spectra presenting two primary peaks at about 3435 cm^{-1} (corresponding to the absorption of stretching of the OH groups) and at 2025 cm^{-1} (corresponding to the C–H stretching of the CH_2 groups). The CO asymmetrical stretching at a maximum of 1609 cm^{-1} along with a weaker symmetrical stretching band at 1414 cm^{-1} [22] were empiric due to the salt nature of carboxylic acid groups in pure Na-Alg. An accelerated band at 1083 cm^{-1} reflects the stretching of C–O–C group; the peaks at 601 cm^{-1} belong to C–O–C glycosidic linkage (ring breathing) [23]. They are accompanying its saccharide structure [24]. In the case of AgNPs, the band of $CO_2{}^-$ shifted to 1613 cm^{-1}, while the peaks of 3435 and 1414 cm^{-1} shifted to 3422 and 1384 cm^{-1}, respectively, due to ring stretching of metal groups and indicating that Na-Alg was doped by $NO_3{}^-$ because of the stabilization of AgNPs. The comparison between the Na-Alg and Na-Alg/AgNPs FT-IR spectra only showed minor changes in position as well as the absorption bands. Therefore, the FT-IR spectrum confirms that AgNPs have been capped with the aid of the lone pair electrons around the oxygen atoms in organic compound in Na-Alg with Van der Waals forces [25]. Figure 1B presents an SEM image of Na-Alg-loaded AgNPs. It is evident that green-synthesized AgNPs can cautiously be admired as nanoparticles with a spherical nature. Due to the interactions of hydrogen bonds and electrostatic interactions between the bioorganic capping molecules bound to the Ag-NPs expose larger as a result of the Ag-NPs agglomeration was revealed [26].

The TEM images with the corresponding particle size distribution (PSD) of the prepared AgNPs are shown in Figure 1D,E. This demonstrates the formation of AgNPs and offers us a clear view of the shape, length, and distribution of the particles in nanoscale. From the image, it can be seen that the located AgNPs are round in form and nicely separated in the aqueous medium, which covers them with a layer. This layer might be the phytoconstituents of Na-Alg. In addition, the aggregation is lower because AgNPs collide less frequently. From the particle size distribution curve, it can be seen that the most of the particles sizes ranging from 6 nm to 10 nm. The reductive properties of Na-Alg are notably more desirable owing to the base hydrolysis with the formation of low molecular weight reducing fragments, consequently reflecting the twin function of Na-Alg as a stabilizing and reducing agent in an alkaline medium [27]. The additional support of the reduction of Ag^+ ions to elemental silver confirmed by EDS analysis is shown in Figure 1F. The optical absorption peak is observed at approximately 3 keV, which is typical for the absorption of metallic silver nanocrystals due to surface plasmon resonance [28], confirming the presence of nanocrystalline elemental silver. An XRD pattern of Na-AgNPs was completed to verify that the crystal phase of the prepared AgNPs fell within the range of 30°–80°. Figure 1G illustrates the typical XRD pattern of the alginate–AgNPs prepared with several distinct diffraction peaks at 38.1°, 44.2°, 64.3°, and 77.4°, which are assigned to reflections from the (111), (200), (220), and (311) planes of the silver crystal, respectively. This confirms the existence of silver; furthermore, they can be indexed as the face-centered-cubic (FCC) structure of silver. These peaks occur due to the crystalline and amorphous natural stages that accompany crystallized AgNPs. In addition to the Bragg peaks representative of FCC silver nanocrystals, additional, and yet unassigned peaks were also observed due to amoebic compounds that were responsible for silver ion reduction and the stabilization of the resultant nanoparticles [29].
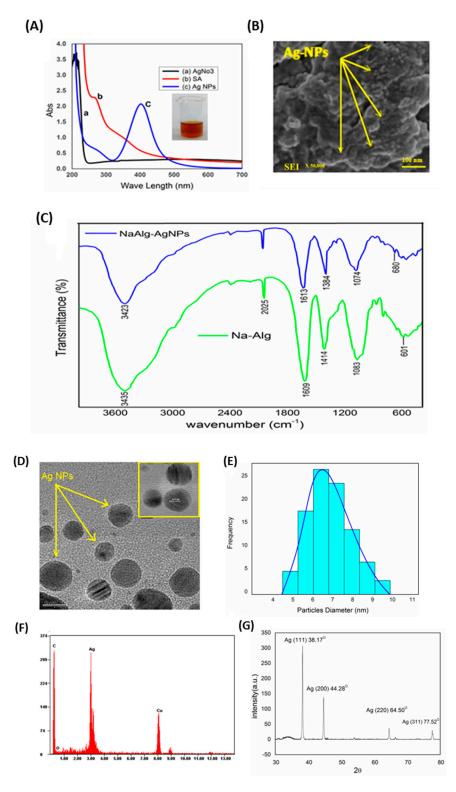
Figure 1. (**A**) UV–vis spectra; (**B**) SEM; (**C**) Fourier transform infrared (FT-IR) spectra; (**D**) TEM; (**E**) particle size distribution (PSD); (**F**) energy dispersive X-ray spectroscopy (EDS); and (**G**) XRD of AgNPs.

3.2. Optimization of Silk Treatment Conditions

The inherent nature of protein-based Bombyx mori silk is amphoteric; an important reason behind this remarkable property is demonstrated by attributing ionizable groups of the side chain of various amino acids that dissociated equilibrium state is influenced by pH conditions [30]. As a result,

this property of silk is responsible for attracting and binding the charged metal ions [31]. When silk was immersed in an aqueous solution of metal salts, it showed the propensity to engross metal cations, while the rate and extent of the uptake depended on several factors, such as the type of metal and its valence state; the pH of the application medium; the time of exhaustion; and the temperature of the application bath. However, the effect of the application medium pH (keeping other parameters constant for 40 min at a temperature of 40 °C) on the AgNPs-treated fabric was investigated. On the absorption of AgNPs, the silk fabric acquired a pale-yellow shade that can be computed by the K/S value of the treated silk fabric. From Figure 2a, it is clear that the K/S values of the treated silk with 35 ppm and 70 ppm AgNPs were 0.4465 and 0.6848, respectively, at pH 4.0, indicating an excellent uptake of AgNPs by the silk. When the AgNPs application medium was more acidic (pH about 3.0), the K/S value of the treated fabric was comparatively less—about 0.3235 and 0.4952 for 35 ppm and 70 ppm AgNPs, respectively. However, in a more alkaline medium (pH 10), the K/S values came to 0.2701 and 0.2857 for silk fabric treated with 35 ppm and 70 ppm AgNPs, respectively, which is very near to the K/S value of the untreated silk, representing a much lower uptake of AgNPs. Some studies have reported that the AgNPs produce a negative zeta potential (-35 mV) around the surface when dispersed in water [32]. Therefore, the low uptake of the AgNPs by the silk fabric at a higher pH could be explained by negative–negative repulsion because the amphoteric nature of the silk fabric developed a stronger negative charge on its surface. Furthermore, due to this very amphoteric nature, the silk fabric becomes more positively charged in a lower pH and hence more easily attracts the negatively-charged AgNPs; this results in higher uptake.
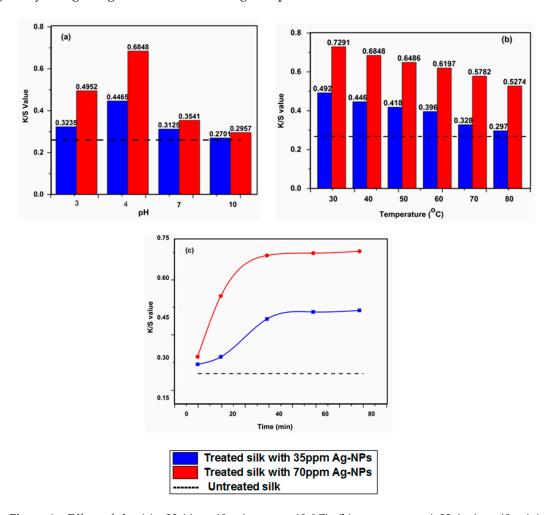

Figure 2. Effect of the (**a**) pH (time 40 min, temp 40 °C); (**b**) temperature (pH 4, time 40 min); and (**c**) effect of the application time (pH 4, temp 40 °C) on the particle uptake in terms of K/S value.

The effect of temperature (keeping other parameters constant for 40 min at pH 4) on the AgNPs uptake was evaluated in terms of the K/S values of the treated silk fabrics; these are shown in Figure 2b. From Figure 2b, it can be observed that the K/S value decreased dramatically with increasing temperature, demonstrating a decrease in the AgNPs uptake. The absorption of AgNPs by the silk sample might be an exothermic interaction, and hereafter any increase in the application temperature results in lower AgNPs uptake. Experiments were repeated several times at each temperature to study the effect of temperature. Therefore, it cannot be accidental that there was an important difference in AgNPs uptake at each temperature level.

The effects of exhaustion time (keeping other parameters constant; at pH 4 and a temperature of 40 °C) of AgNPs on the silk fabric in terms of the K/S value can be seen in Figure 2c. The figure reveals that the K/S value increased between 10 and 40 min. This is due to the changing pattern of the silk materials and the zeta potential of the AgNPs. The silk surface had a positive charge and AgNPs surface had a negative charge, which resulted in a strong attraction between them. Therefore, the rate of Ag-NPs uptake was very high at 40 min and beyond this time no significant change was appeared in the curve and can be considered as asymptotic behavior up to the 80 min.

3.3. Absorption Characteristics

The UV–vis absorption spectrum of the solution of AgNPs before and after coating is presented in Figure 3A. It can be noticed that the absorbance units of the 70 ppm AgNPs solution was higher than the 35 ppm AgNPs solution after coating. This could be due to the high affinity of the silk, which is sufficient to adsorb nearly all Ag+ and AgNPs present. This shows that silk fabric has a better absorption capability for AgNPs in an alkaline environment. This can be explained by the decreased repulsion forces between the negatively-charged AgNPs and the silk fibers. The colors of the treated fabrics that emerged were associated with the surface plasmon resonance (SPR) properties of green-synthesized AgNPs. In order to analyze the SPR of AgNPs on the treated fabric, the absorption traits of the 35 and 70 ppm AgNPs-treated fabrics were evaluated using a spectrophotometer within the range of 200 and 800 nm, as shown in Figure 3B. From this figure, it is clear that the control fabric had no absorption spectra. On the contrary, the AgNPs-treated fabric exhibited an absorption band located in the range of 410–470 nm, which indicates the presence of the surface plasmon absorption band of AgNPs; these after-effects enhanced the depositing of green-synthesized AgNPs on the silk.
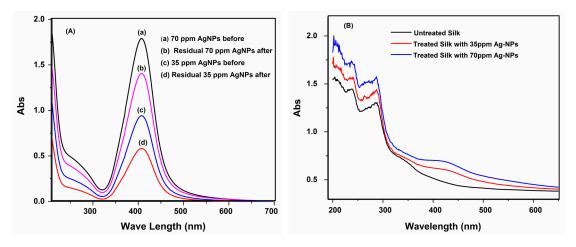

Figure 3. UV–vis spectra: (**A**) for residual Ag NPs solution with before and after treatment; and (**B**) the untreated and AgNPs-treated fabrics.

3.4. FT-IR and XRD Analysis

FT-IR spectral analysis was performed to observe the growth of polymer and AgNPs on the silk fabrics. Figure 4A, (a), (b), and (c) show the FT-IR spectra of both untreated and AgNPs-treated

(35 ppm and 70 ppm, respectively) fabric samples. Figure 4A (a) shows the FT-IR spectrum of silk that is characterized by strong bands over 3000 cm^{-1} (due to OH and NH stretching vibrations) and various amide bands at 1550, 1250, and 650 cm^{-1} (from stretching vibrations of CN and NH deformation vibrations), which are typical of polypeptides and proteins and allow their conformational characterization [33]. Compared with the FT-IR spectrum of the untreated silk fabric, the spectrum of the silver-coated silk fabric also has these characteristic peaks, making it possible to observe the chelation between silk and silver. Subfigures (b) and (c) from Figure 4A show the –NH$_2$ group at 3200 cm^{-1} (stretching frequency of the C=O) after the modification of AgNPs, which demonstrates that it successfully bound to the fabric. This shift occurs because of the reduction of the double bond character of the C=O, which is due to the synchronization of oxygen to the metal center and is in accordance with the effects caused by the added complexes defined previously [34].

Silk fibroin is known to be crystalline and accelerates the X-ray diffraction pattern. Figure 4B (a), (b), and (c) show the XRD spectra of untreated and Ag nanoparticles (35 ppm and 70 ppm, respectively) treated fabric samples. Figure 4B, (a) provides the XRD spectra of pristine silk fabric that shows a strong diffraction peak (2θ = 20.7°), a weak diffraction peak (2θ = 24.5°), and two shoulder diffraction peaks (2θ = 28.8° and 40.0°). These XRD diffraction peaks are attributed to the β-sheet structure of native silk [35], indicating the high crystallinity of pristine silk fabric. Compared with this, the XRD pattern of the treated silk exhibited five new XRD peaks with 2θ = 38.4°, 44.6°, 64.8°, 77.8°, and 81.9° (Figure 4B), which can be ascribed to (111), (200), (220), (311), and (222) planes of the face-centered cubic (FCC) lattice of silver (JCPDS card. No. 4-0783) [36]. The peaks are broadened due to the small size of NPs. Finally, from the XRD spectra it is possible to conclude that the crystalline nature of the untreated and treated samples was not altered by AgNPs, which could be clarified further by the fact that the Bragg's angle is the same for both samples.
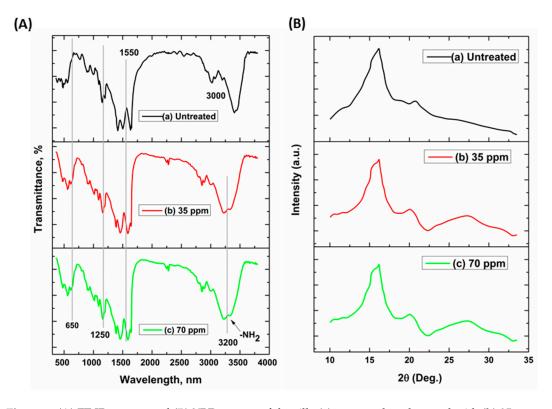

Figure 4. (**A**) FT-IR spectra and (**B**) XRD spectra of the silk; (**a**) untreated, and treated with (**b**) 35 ppm and (**c**) 70 ppm AgNPs at optimized condition.

3.5. Thermal Properties

The thermal behavior of the control and AgNPs-treated fabrics was tested by thermo-gravimetric analysis (TGA); the results are shown in Figure 5A. The degradation temperature—known as a standard of thermal degradation—was measured based on the TGA curves. Figure 5A, (a), (b), and (c) illustrate the TGA curves of the control (untreated) and the Ag nanoparticles (35 ppm and 70 ppm, respectively) treated silk samples, with two peak temperatures and three successive stages of weight loss. The initial weight loss of the control and AgNPs-treated samples came to about 5.5% and 4.5%, respectively, until about 198 °C. As stated previously, these weight changes could be explained by the removal of adsorbed water [37]. Due to the hydrophilic nature of silk, it was subjected to a dehydration process, in which absorbed or crystal water was removed, and the color turned yellow. A weight loss of about 50% and 57% was observed in the control silk and the AgNPs-treated sample respectively, in the temperature range of 290–500 °C, which can be associated with the breakdown of the side chain groups of the silk structure [38]. Another substantial weight loss of about 23% occurred in the 500–650 °C range for both samples, and can be attributed to the breakdown of the main chain groups of silk fibroin, as reported previously [39]. The mass loss in the first stage of the TG curves (200–300 °C) is due to the moisture evaporating from the silk. The moisture content (%) of the silk treated with nanoparticles is shown in Figure 5B. It can be observed that loading the material with nanoparticles led to an increase in the moisture content of the silk since the silk treated with AgNPs (70 ppm AgNPs) presented the highest moisture content (7%). This results are in good agreement with the results of silver content is shown in physical properties of samples.
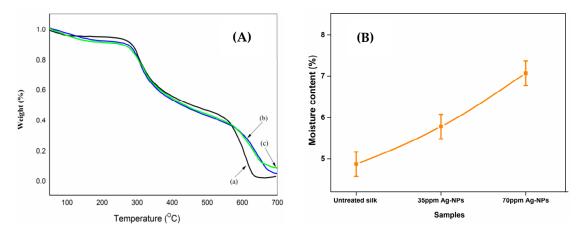

Figure 5. (**A**) Thermo-gravimetric analysis (TGA) curve: (**a**) control silk; and treated silk with (**b**) 35 ppm AgNPs and (**c**) 70 ppm AgNPs. (**B**) Moisture content (%).

3.6. Scanning Electron Microscope (SEM)

The surface morphologies of the treated fabrics were observed by SEM in order to observe the assembly of AgNPs on the fabric surface. The SEM micrographs are shown in Figure 6. Figure 6a shows the pristine fabric morphology with a typically smooth longitudinal fibril surface structure. The morphologies of fabrics with AgNPs incorporated are shown in Figure 6b,c. It can be seen that a uniform layer of nano-sized Ag was only deposited on both fabrics' surfaces, which indicates that the morphologies of treated fabrics were not damaged during the functionalization process of the AgNPs, and the coloration of silk was influenced by this behavior of AgNPs on the fiber surface.
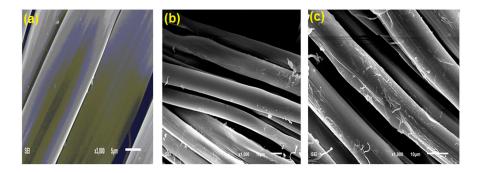
Figure 6. SEM micrographs of (**a**) control silk and silk treated at (**b**) 35 ppm and (**c**) 70 ppm AgNPs.

3.7. Color Measurements and Fastness

The color characteristics (i.e., K/S values, L*, A*, and B*) of the silk coated with AgNPs are listed in Table 1. Typically, by measuring color strength (K/S) values, the amount of dye as a percentage of the colored fabric can be determined, where a higher K/S value shows greater color intensity, indicating a greater amount of AgNPs incorporated in the fabric. The results reveal that all K/S values of the silk samples with AgNPs included were notably higher than the untreated ones; this is due to the formation of AgNPs that cause coloration trait of the material. The lightness (L*) of silver-coated silk samples was lower than that of the original silk, while A* and B* values increased dramatically. Positive A* and B* values were obtained for all treated fabric samples; this is because the modified fabrics appeared yellowish-brown in color (Figure 7). The different color of the treated fabrics could be due to the formation of large discrete particles and the aggregation of small particles. The absorption of AgNPs relies significantly on the form, length, and application media and varying synthesis conditions can influence these characteristics [40]. Therefore, increasing the concentration of AgNPs can affect the absorption features of the loaded AgNPs, but might not confirm any correlation between the color strength of the treated silk and the Ag content. It was observed that the K/S value can be a measure of the concentration of deposited AgNPs on the fabric due to the unique optical properties of AgNPs [41]. In Table 1, it is possible to see that washing- and light-fastness properties range from good to very good. It was observed that due to the presence of chemical linkage (i.e., Van der Waals forces) in the Ag NPs-treated fabrics, they showed good fastness properties.

Table 1. Color coordinate data (CIE Lab) and K/S values of untreated and AgNPs-treated silk.

Sample	L*	A*	B*	K/S	CFL [1]	CFW [2]
Untreated silk	89.97	−0.07	8.54	0.2603	-	-
35 ppm AgNPs	83.68	1.72	15.43	0.4465	6	4–5
70 ppm AgNPs	81.93	0.77	22.23	0.6848	6	4–5

[1] Colorfastness to light; [2] Colorfastness to wash.
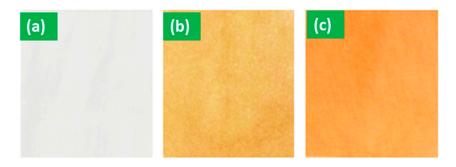

Figure 7. Photographs of (**a**) control silk, and AgNPs-treated fabric with (**b**) 35 ppm and (**c**) 70 ppm.

3.8. UV Protection

The ultraviolet radiation (UVR) band consists of three regions: the UV-A band (320–400 nm); the UV-B band (290–320 nm); and the UV-C band (200–290 nm). The damage to human skin from UV radiation occurs in the range of UV-A. Recently, metal nanoparticles and metal salts have been used as UV protecting agents [42]. Therefore, the effect of green-based AgNPs on the optical properties of fabrics—specifically, the UV transmittance of untreated and treated silk samples—was measured using UV transmittance spectroscopy at the wavelength range between 200 and 440 nm (Figure 8a). The transmittance spectra of all samples demonstrated obvious differences. Typically, the untreated silk showed the highest percentage of UV transmittance compared to those treated, which suggests that silk fabric had no significant effect on UV protection properties. Once the silk was functionalized with 35 ppm AgNPs, the corresponding spectrum of AgNPs-treated silk decreased to about 46% in comparison with the raw silk fabric. It was found that the incorporation of 70 ppm AgNPs on fabric-treated clearly reduced UV transmittance to 84%, suggesting that AgNPs offer high protection from UV rays. These results indicate the ability of the AgNPs-treated fabrics to block UV rays from passing through and reaching the skin. The high UV protection levels of the finished fabrics with incorporated AgNPs could come about due to the large refractive index of AgNPs, resulting in very efficient UV scattering [43]. Previous studies have revealed that AgNPs enhance the UV protection property of fabric due to the plasmon structure of AgNPs [44]. Therefore, our results indicate that green-based AgNPs absorb UV rays, which is consistent with previous findings.
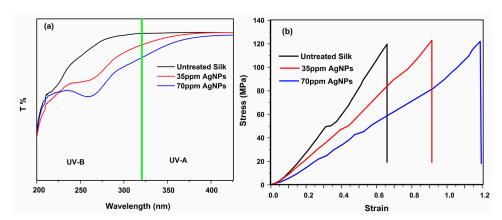

Figure 8. (**a**) UV transmission spectra and (**b**) stress–strain curve for the untreated and AgNPs-treated fabrics.

3.9. Antibacterial Activity

The bacterial inhibition efficiency of AgNPs-treated fabrics was investigated using the zone of inhibition test, which is a qualitative analysis involving an agar diffusion test. To examine the antibacterial efficacy of the samples, bacteria-inoculated agar plates were used as media, as shown in Figure 9. Bacterial growth was noted by evaluating the size of the diameter of zones of inhibition around silk treated with a commercial antibacterial agent, and fabric treated with green-synthesized AgNPs (Table 2), thus investigating the inhibitory effect of green-based AgNPs. The inhibition zone test results in Figure 9 clearly show that the commercial antibacterial agent displayed the largest inhibition zones for *E. coli* (24 ± 1.04) and *S. aureus* (29 ± 0.52). The AgNPs-treated fabrics also showed very obvious inhibition zones around the specimen, and the diameter of each transparent zone was close to the commercial sample. The concentrations of AgNPs played a vital role in certifying the zone of inhibition results. As shown in Table 2, there were more silver ions when the fabric was functionalized using 70 ppm AgNPs, yielding a sample which exhibited a better inhibitory effect against both microorganisms with a zone of inhibition up to 23 ± 0.38 mm in diameter for *E. coli* and 26 ± 0.46 mm in diameter for *S. aureus*; whereas the sample with 35 ppm AgNPs established zones of inhibition up to 22 ± 0.44 mm in diameter for *E. coli* and 24 ± 0.66 mm in diameter for

S. aureus. This phenomenon was attributed to the mechanism of biocidal action of the fabric enhanced by the leaching of Ag$^+$ ions [45]. In addition, AgNPs are extremely reactive with proteins because they adversely affect cellular metabolism electron transfer systems and strongly inhibit the substrate transportation into cell membranes when these nanoparticles come in to contact with bacteria and fungi responsible for infection, odor, itchiness, and sores. A quantitative assessment of the antibacterial activity of functionalized silk with synthesized green-based AgNPs was also performed according to the percentage reduction method (AATCC 100) shown in Table 2. AgNPs have a significant effect on bacterial reduction; both concentrations of AgNPs caused the inhibition rate to increase to above 90%. When the concentration of AgNPs increased, antibacterial activity against *E. coli* and *S. aureus* improved slowly and stably. This can be described in terms of a certain degree of a sterilizing effect due to the presence of metallic ions, as well as metallic compounds. Perhaps a segment of atmospheric oxygen in water or air is transformed into active oxygen due to the catalysis of metallic ion, thereby dissolving the organic substance to enhance sterilizing action [46]. Furthermore, AgNPs are able to increase their contact with microbes because of their extremely large relative surface area, which results in the enhancement of antimicrobial success. The antibacterial performance demonstrated in the above experiments is perfectly in agreement with the broad spectrum of antimicrobial activity of AgNPs, showing that this could be a good competitor for conventional antibacterial agents.
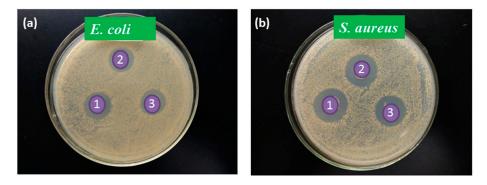

Figure 9. Antibacterial activity of (**1**) the commercial and AgNPs-treated fabrics (**2**) 35 ppm, (**3**) 70 ppm on (**a**) *E. coli* and (**b**) *S. aureus*.

Table 2. Antibacterial activity of silk fabric coated with green-based AgNPs.

Samples	Bacterial Reduction (%)		Zone of Inhibition (mm)	
	E. coli	*S. aureus*	*E. coli*	*S. aureus*
Commercial	95 ± 2.2	97 ± 4.2	24 ± 1.04	29 ± 0.52
35 ppm AgNPs	88 ± 1.10	91 ± 2.08	22 ± 0.44	24 ± 0.66
70 ppm AgNPs	90 ± 2.12	94 ± 4.06	23 ± 0.38	26 ± 0.46

Values represent means ± standard deviations from three experiments.

3.10. Surface Wettability

The wettability of all fabric samples with water was measured by taking obvious contact angle measurements. As the thermodynamic property that characterizes the wettability of solid surfaces, the contact angle is of utmost importance in modern technological applications and materials science. Contact angles are sensitive to many factors, such as surface geometry, roughness, contamination, deformation, etc. Such sensitivity enables the detection of very small-scale outcomes via this macroscopic measurement [47]. When the water contact angle is smaller than 90°, the surface is identified as hydrophilic; if the water contact angle is larger than 90°, the surface is called hydrophobic. The data on the contact angle measurements is shown in Figure 10. These results depict the evolution of water droplets on the surface of the silk samples over time, indicating that the water droplets on

untreated silk disappeared rapidly with respect to the behavior of water droplets on the treated sample. The contact angle of the untreated silk fabric was 0° after 10 s. Similarly, the water droplets on the surface of AgNPs-treated silk fabric disappeared within 20 s. This clearly shows that AgNPs-coating significantly increased the surface contact angle of the silk fabric. The greater water contact angle exhibited by the AgNPs-treated samples implies that the hydrophobic property of silk fabric was improved. This can be attributed to the formation of stable chemical structures on the fabric surface after AgNPs coating. Compared with untreated silk fabric, the slower change rate of water droplets on the AgNPs-treated silk suggests that the assembly of AgNPs increased the hydrophobicity of the silk.
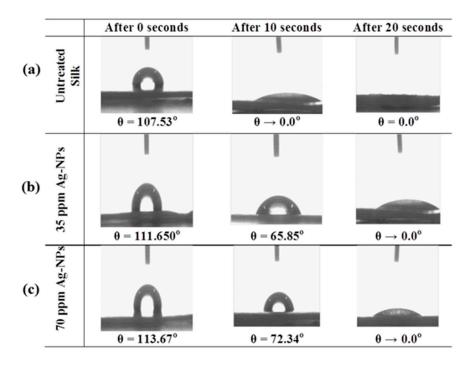

Figure 10. Water contact angles on the silk fabric surface, before and after washing.

3.11. Mechanical Properties

Figure 8b demonstrates the tensile behavior of silk samples treated with AgNPs of different concentrations. The analysis of the stress–strain curve indicates that the AgNPs-treated silk samples exhibited the same elasticity and then continuously hardened until final failure. The diagrams show that the tensile force for the silk sample treated with AgNPs was up to 2.50% more than that of the untreated one. Based on this result, it can be concluded that the Na-Alg-stabilized AgNPs-treated silk sample improved the mechanical properties of the fabric. The reason for this may be that the intercalation nature of silver helps to disperse nanoparticles in the silk fiber which undergoes slippage under tensile loading [48]. Another explanation could be attributed to the fact that the particle size is in the nano range, allowing the AgNPs to enter in between the polymer structure and thus possibly functioning as a filler or crosslinking agent, further contributing to the load shearing phenomenon during the application of load to the material. This result is in agreement with previous research [49]. The loss of strength due to the treatment is around 20%, and as such, the observed loss in strength lies well within the reported values and is accepted in the industry.

3.12. Physical Properties

Table 3 gives the data on the various physical properties of the treated fabric at varying concentrations of AgNPs. There was slight improvement in crease recovery angle of AgNPs-treated silk fabric with a small increase in bending length. This phenomenon confirms that the particles

slipping between the polymer molecules do not contribute much to the overall polymer flexibility. The behavior is thus devoid of harshness to the materials. No distinct change could be felt by hand between untreated and AgNPs-treated silk; all the silk samples felt equally soft and smooth. To further observe the influences of the assembly of AgNPs on the handling of the silk, bending lengths were measured (Table 3). Since fabric bending length is related to fabric stiffness or handling, these results suggest that the assembly of AgNPs did not change the handling of the silk samples, as the size of AgNPs lies in nano range. The effects of the AgNPs on the yellowness of silk samples treated with AgNPs are also described in Table 3. It is clear that the green-synthesized AgNPs caused a slight yellowing compared with the untreated silk fabric. The untreated silk fabric sample had the lowest yellowness, while the fabric sample treated with the highest AgNPs concentration also had the highest yellowness index value (82 for 70 ppm AgNPs). This might result from pyrolysis and oxidation of the surface components [50].

Table 3. Physical properties of samples.

Samples	Ag Content (mg/kg)	CRA (deg)	Bending Length (cm)	Yellowness Index
Untreated Silk	-	124	2.30	22
35 ppm AgNPs-treated Silk	7125 ± 15	132 (±6.02)	2.46 (±6.00)	65
70 ppm AgNPs-treated Silk	8362 ± 23	135 (±5.55)	2.53 (±5.02)	82

4. Conclusions

The present paper proposed a novel approach to the functionalization of "Rajshahi silk fabric" by an exhaustive method through the green synthesis of AgNPs for the first time. The FT-IR spectra confirmed the presence of functional groups, while TEM image and XRD data reveal that the synthesized AgNPs possess good crystalline structures. SEM studies showed that the AgNPs were well-deposited on the fiber surface, while the residue weight observed in the TGA experiment further proved the successful synthesis of AgNPs on the silk fiber surface. The effects of pH, time, and temperature were also studied while AgNPs were applied on silk, where optimized conditions were determined at pH 4, and 40 °C for 40 min. AgNPs treatment enhanced the color strength of silk and also improved the fastness towards light and washing, which suggests this method can overcome the limitations of traditional dyeing processes. The treatment with AgNPs improved the fabric's tensile properties and crease recovery angle, with almost no effect on the rigidity of the material. The results of the bacterial test confirmed that the proposed method is highly effective for antibacterial action, as the antibacterial activity increased with increasing concentration of AgNPs on the fiber surface.

Author Contributions: S.M. and H.-H.L. conceived the paper; S.M. designed and performed the experiments; M.Z.S. performed the wettability experiments; M.N.P. performed the XRD experiments; M.A.H. performed the TGA experiments; S.M. and M.N.P. wrote the paper; and all the authors reviewed and edited the final paper.

References

1. Dubey, S.P.; Lahtinen, M.; Särkkä, H.; Sillanpää, M. Bioprospective of sorbus aucuparia leaf extract in development of silver and gold nanocolloids. *Colloids Surf. B* **2010**, *80*, 26–33. [CrossRef] [PubMed]

2. Chen, W.; Yan, J.; Song, N.; Li, Q.; Yang, B.; Dai, Y. Study on silver nanopowder prepared by chemical reduction with an organic reductant. *Guijinshu (Pre. Met.)* **2006**, *27*, 14–17.

3. Choi, N.; Seo, D.; Lee, J. Preparation and stabilization of silver colloids protected by surfactant. *Mater. Sci. For.* **2005**, *29*, 394–396.

4. Jiangmei, Y.; Huiwang, T.; Muling, Z.; Jun, T.; Zhang, S.; Zhiying, Y.; Wei, W.; Jiaqiang, W. PVP-capped silver nanoparticles as catalyst for oxidative coupling of thiols to disulfides. *Chin. J. Catal.* **2009**, *30*, 856–858.

5. Setua, P.; Chakraborty, A.; Seth, D.; Bhatta, M.U.; Satyam, P.; Sarkar, N. Synthesis, optical properties, and surface enhanced raman scattering of silver nanoparticles in nonaqueous methanol reverse micelles. *J. Phys. Chem. C* **2007**, *111*, 3901–3907. [CrossRef]

6. Bonilla, J.J.A.; Guerrero, D.J.P.; Sáez, R.G.T.; Ishida, K.; Fonseca, B.B.; Rozental, S.; López, C.C.O. Green synthesis of silver nanoparticles using maltose and cysteine and their effect on cell wall envelope shapes and microbial growth of *Candida* spp. *J. Nanosci. Nanotechnol.* **2017**, *17*, 1729–1739. [CrossRef]

7. Wei, D.; Sun, W.; Qian, W.; Ye, Y.; Ma, X. The synthesis of chitosan-based silver nanoparticles and their antibacterial activity. *Carbohydr. Res.* **2009**, *344*, 2375–2382. [CrossRef] [PubMed]

8. Park, Y.; Hong, Y.; Weyers, A.; Kim, Y.; Linhardt, R. Polysaccharides and phytochemicals: A natural reservoir for the green synthesis of gold and silver nanoparticles. *IET Nanobiotechnol.* **2011**, *5*, 69–78. [CrossRef] [PubMed]

9. Yang, J.; Chen, S.; Fang, Y. Viscosity study of interactions between sodium alginate and ctab in dilute solutions at different ph values. *Carbohydr. Polym.* **2009**, *75*, 333–337. [CrossRef]

10. Tønnesen, H.H.; Karlsen, J. Alginate in drug delivery systems. *Drug Dev. Ind. Pharm.* **2002**, *28*, 621–630. [CrossRef] [PubMed]

11. Darroudi, M.; Ahmad, M.B.; Abdullah, A.H.; Ibrahim, N.A.; Shameli, K. Effect of accelerator in green synthesis of silver nanoparticles. *Int. J. Mol. Sci.* **2010**, *11*, 3898–3905. [CrossRef] [PubMed]

12. Lu, Z.; Xiao, J.; Wang, Y.; Meng, M. In situ synthesis of silver nanoparticles uniformly distributed on polydopamine-coated silk fibers for antibacterial application. *J. Colloid Interface Sci.* **2015**, *452*, 8–14. [CrossRef] [PubMed]

13. Sheikh, M.R.K.; Farouqui, A.N.; Yahya, R.; Hassan, A. Effect of acid modification on dyeing properties of rajshahi silk fabric with different dye classes. *Fibers Polym.* **2011**, *12*, 642–647. [CrossRef]

14. Zhang, D.; Toh, G.W.; Lin, H.; Chen, Y. In situ synthesis of silver nanoparticles on silk fabric with PNP for antibacterial finishing. *J. Mater. Sci.* **2012**, *47*, 5721–5728. [CrossRef]

15. Naik, R.; Wen, G.; Hureau, S.; Uedono, A.; Wang, X.; Liu, X.; Cookson, P.G.; Smith, S.V. Metal ion binding properties of novel wool powders. *J. Appl. Polym. Sci.* **2010**, *115*, 1642–1650. [CrossRef]

16. Yin, H.; Ai, S.; Shi, W.; Zhu, L. A novel hydrogen peroxide biosensor based on horseradish peroxidase immobilized on gold nanoparticles–silk fibroin modified glassy carbon electrode and direct electrochemistry of horseradish peroxidase. *Sens. Actuators B* **2009**, *137*, 747–753. [CrossRef]

17. Gulrajani, M.; Gupta, D.; Periyasamy, S.; Muthu, S. Preparation and application of silver nanoparticles on silk for imparting antimicrobial properties. *J. Appl. Polym. Sci.* **2008**, *108*, 614–623. [CrossRef]

18. Pervez, M.N.; Rahman, M.A.; Yu, L.; Cai, Y. A novel study on uv protection and antibacterial properties of washed denim garment. *MATEC Web Conf.* **2017**, *108*, 03004. [CrossRef]

19. Slistan-Grijalva, A.; Herrera-Urbina, R.; Rivas-Silva, J.; Ávalos-Borja, M.; Castillón-Barraza, F.; Posada-Amarillas, A. Classical theoretical characterization of the surface plasmon absorption band for silver spherical nanoparticles suspended in water and ethylene glycol. *Phys. E Low-Dimen. Syst. Nanostruct.* **2005**, *27*, 104–112. [CrossRef]

20. Stamplecoskie, K.G.; Scaiano, J.C. Light emitting diode irradiation can control the morphology and optical properties of silver nanoparticles. *J. Am. Chem. Soc.* **2010**, *132*, 1825–1827. [CrossRef] [PubMed]

21. Abdel-Halim, E.; Al-Deyab, S.S. Utilization of hydroxypropyl cellulose for green and efficient synthesis of silver nanoparticles. *Carbohydr. Polym.* **2011**, *86*, 1615–1622. [CrossRef]

22. Manuja, A.; Kumar, S.; Dilbaghi, N.; Bhanjana, G.; Chopra, M.; Kaur, H.; Kumar, R.; Manuja, B.K.; Singh, S.K.; Yadav, S.C. Quinapyramine sulfate-loaded sodium alginate nanoparticles show enhanced trypanocidal activity. *Nanomedicine* **2014**, *9*, 1625–1634. [CrossRef] [PubMed]

23. Cardenas-Jiron, G.; Leal, D.; Matsuhiro, B.; Osorio-Roman, I. Vibrational spectroscopy and density functional theory calculations of poly-D-mannuronate and heteropolymeric fractions from sodium alginate. *J. Raman Spectrosc.* **2011**, *42*, 870–878. [CrossRef]

24. Sartori, C.; Finch, D.S.; Ralph, B.; Gilding, K. Determination of the cation content of alginate thin films by FTi.r. Spectroscopy. *Polymer* **1997**, *38*, 43–51. [CrossRef]

25. Mandal, A.; Sekar, S.; Chandrasekaran, N.; Mukherjee, A.; Sastry, T.P. Vibrational spectroscopic investigation on interaction of sago starch capped silver nanoparticles with collagen: A comparative physicochemical study using ft-ir and ft-raman techniques. *RSC Adv.* **2015**, *5*, 15763–15771. [CrossRef]

26. Devaraj, P.; Kumari, P.; Aarti, C.; Renganathan, A. Synthesis and characterization of silver nanoparticles using cannonball leaves and their cytotoxic activity against mcf-7 cell line. *J. Nanotechnol.* **2013**, *2013*, 1–5. [CrossRef]

27. El-Rafie, M.; El-Naggar, M.; Ramadan, M.; Fouda, M.M.; Al-Deyab, S.S.; Hebeish, A. Environmental synthesis of silver nanoparticles using hydroxypropyl starch and their characterization. *Carbohydr. Polym.* **2011**, *86*, 630–635. [CrossRef]

28. Mohammed Fayaz, A.; Balaji, K.; Girilal, M.; Kalaichelvan, P.; Venkatesan, R. Mycobased synthesis of silver nanoparticles and their incorporation into sodium alginate films for vegetable and fruit preservation. *J. Agric. Food Chem.* **2009**, *57*, 6246–6252. [CrossRef] [PubMed]

29. Roopan, S.M.; Madhumitha, G.; Rahuman, A.A.; Kamaraj, C.; Bharathi, A.; Surendra, T. Low-cost and eco-friendly phyto-synthesis of silver nanoparticles using cocos nucifera coir extract and its larvicidal activity. *Ind. Crop. Prod.* **2013**, *43*, 631–635. [CrossRef]

30. Arai, T.; Freddi, G.; Colonna, G.; Scotti, E.; Boschi, A.; Murakami, R.; Tsukada, M. Absorption of metal cations by modified *B. mori* silk and preparation of fabrics with antimicrobial activity. *J. Appl. Polym. Sci.* **2001**, *80*, 297–303. [CrossRef]

31. Li, G.; Liu, H.; Li, T.; Wang, J. Surface modification and functionalization of silk fibroin fibers/fabric toward high performance applications. *Mater. Sci. Eng. C* **2012**, *32*, 627–636. [CrossRef]

32. Sur, I.; Altunbek, M.; Kahraman, M.; Culha, M. The influence of the surface chemistry of silver nanoparticles on cell death. *Nanotech* **2012**, *23*, 375102. [CrossRef] [PubMed]

33. Arai, T.; Freddi, G.; Innocenti, R.; Kaplan, D.; Tsukada, M. Acylation of silk and wool with acid anhydrides and preparation of water-repellent fibers. *J. Appl. Polym. Sci.* **2001**, *82*, 2832–2841. [CrossRef]

34. Ma, Y.; Zhou, T.; Zhao, C. Preparation of chitosan–nylon-6 blended membranes containing silver ions as antibacterial materials. *Carbohydr. Res.* **2008**, *343*, 230–237. [CrossRef] [PubMed]

35. Tao, W.; Li, M.; Zhao, C. Structure and properties of regenerated antheraea pernyi silk fibroin in aqueous solution. *Int. J. Biol. Macromol.* **2007**, *40*, 472–478. [CrossRef] [PubMed]

36. Chang, S.; Kang, B.; Dai, Y.; Chen, D. Synthesis of antimicrobial silver nanoparticles on silk fibers via γ-radiation. *J. Appl. Polym. Sci.* **2009**, *112*, 2511–2515. [CrossRef]

37. Zhang, H.; Magoshi, J.; Becker, M.; Chen, J.Y.; Matsunaga, R. Thermal properties of bombyx mori silk fibers. *J. Appl. Polym. Sci.* **2002**, *86*, 1817–1820. [CrossRef]

38. Lee, S.M.; Cho, D.; Park, W.H.; Lee, S.G.; Han, S.O.; Drzal, L.T. Novel silk/poly (butylene succinate) biocomposites: The effect of short fibre content on their mechanical and thermal properties. *Compos. Sci. Technol.* **2005**, *65*, 647–657. [CrossRef]

39. Asakura, T. Structural characteristics of silk fibroin and the application as enzyme-immobilized material. *Bioindustry* **1987**, *4*, 878–886.

40. Shin, H.S.; Yang, H.J.; Kim, S.B.; Lee, M.S. Mechanism of growth of colloidal silver nanoparticles stabilized by polyvinyl pyrrolidone in γ-irradiated silver nitrate solution. *J. Colloid Interface Sci.* **2004**, *274*, 89–94. [CrossRef] [PubMed]

41. Mowafi, S.; Rehan, M.; Mashaly, H.M.; Abou El-Kheir, A.; Emam, H.E. Influence of silver nanoparticles on the fabrics functions prepared by in-situ technique. *J. Text. Inst.* **2017**, *108*, 1–12. [CrossRef]

42. Emam, H.E.; Bechtold, T. Cotton fabrics with uv blocking properties through metal salts deposition. *Appl. Surf. Sci.* **2015**, *357*, 1878–1889. [CrossRef]

43. Gorenšek, M.; Recelj, P. Nanosilver functionalized cotton fabric. *Text. Res. J.* **2007**, *77*, 138–141. [CrossRef]

44. Xue, C.-H.; Chen, J.; Yin, W.; Jia, S.-T.; Ma, J.-Z. Superhydrophobic conductive textiles with antibacterial property by coating fibers with silver nanoparticles. *Appl. Surf. Sci.* **2012**, *258*, 2468–2472. [CrossRef]

45. Maneerung, T.; Tokura, S.; Rujiravanit, R. Impregnation of silver nanoparticles into bacterial cellulose for antimicrobial wound dressing. *Carbohydr. Polym.* **2008**, *72*, 43–51. [CrossRef]

46. Saito, M. Antibacterial, deodorizing, and uv absorbing materials obtained with zinc oxide (ZnO) coated fabrics. *J. Coat. Fabr.* **1993**, *23*, 150–164. [CrossRef]

47. Drelich, J.; Marmur, A. Physics and applications of superhydrophobic and superhydrophilic surfaces and coatings. *Surf. Innov.* **2014**, *2*, 211–227. [CrossRef]

48. Munakata, M.; Liu, S.Q.; Konaka, H.; Kuroda-Sowa, T.; Suenaga, Y.; Maekawa, M.; Nakagawa, H.; Yamazaki, Y. Syntheses, structures, and properties of intercalation compounds of silver (I) complex with [2.2] paracyclophane. *Inorg. Chem.* **2004**, *43*, 633–641. [CrossRef] [PubMed]
49. Corona-Gomez, J.; Chen, X.; Yang, Q. Effect of nanoparticle incorporation and surface coating on mechanical properties of bone scaffolds: A brief review. *J. Funct. Biomater.* **2016**, *7*, 18. [CrossRef] [PubMed]
50. Yuen, C.; Kan, C. Influence of low temperature plasma treatment on the properties of ink-jet printed cotton fabric. *Fibers Polym.* **2007**, *8*, 168–173. [CrossRef]